

# Growth and piezoelectric properties of $\text{Pb}(\text{Yb}_{1/2}\text{Nb}_{1/2})\text{O}_3\text{--PbTiO}_3$ epitaxial films

Takeshi Yoshimura and Susan Trolier-McKinstry

Materials Research Institute, The Pennsylvania State University, University Park, Pennsylvania 16802

(Received 18 January 2002; accepted for publication 15 July 2002)

Epitaxial films of  $(1-x)\text{Pb}(\text{Yb}_{1/2}\text{Nb}_{1/2})\text{O}_3-x\text{PbTiO}_3$  (PYbN-PT,  $x=0.4,0.5$ ) with  $\text{SrRuO}_3$  bottom electrodes were prepared on (100)  $\text{LaAlO}_3$ , (100)  $\text{SrTiO}_3$ , and (111)  $\text{SrTiO}_3$  substrates by pulsed laser deposition. It was found that vacuum annealing of the  $\text{SrRuO}_3$  before the deposition of PYbN-PT facilitated growth of perovskite PYbN-PT. With optimized growth conditions, (001) and (111) PYbN-PT epitaxial films with good phase purity were obtained in a range of 650–660 and 600–620 °C, respectively. The ferroelectric and transverse piezoelectric properties of these PYbN-PT films were investigated. In the (001) PYbN-PT (50/50) film, the highest remanent polarization ( $\sim 30 \mu\text{C}/\text{cm}^2$ ) and  $e_{31f}$  piezoelectric coefficient ( $-14 \text{C}/\text{m}^2$ ) were observed. The transition temperature of the (001) PYbN-PT (50/50) film was near 380 °C. © 2002 American Institute of Physics. [DOI: 10.1063/1.1505997]

## I. INTRODUCTION

The development of appropriate processing technologies has led to considerable interest in microelectromechanical systems (MEMS).<sup>1–3</sup> Piezoelectric thin films are one means of incorporating sensing and actuation functions in MEMS devices. Ferroelectric films are especially attractive, since films such as  $\text{Pb}(\text{Zr},\text{Ti})\text{O}_3$  (PZT) possess larger piezoelectric charge coefficients than (001)  $\text{ZnO}$  and  $\text{AlN}$  films. Therefore, PZT films have been widely studied and a number of devices using PZT films have been fabricated.<sup>4–6</sup> The reported piezoelectric properties for PZT films, however, appear to be limited to those of hard PZT ceramics. It is known that approximately half of the piezoelectric response of soft PZT ceramics is from extrinsic contributions which are attributed to non-180° domain wall motion.<sup>7–9</sup> In thin films, however, it is believed that non-180° domain wall motion is limited due to small grain size, clamping by the substrate, high defect concentration, etc.

Recently, very large piezoelectric responses have been reported in single crystals of relaxor ferroelectric- $\text{PbTiO}_3$  solid solutions such as  $\text{Pb}(\text{Mg}_{1/3}\text{Nb}_{2/3})\text{O}_3\text{--PbTiO}_3$  (PMN-PT) and  $\text{Pb}(\text{Zn}_{1/3}\text{Nb}_{2/3})\text{O}_3\text{--PbTiO}_3$  (PZN-PT).<sup>10</sup> In rhombohedral crystals, a piezoelectric  $d_{33}$  coefficient of  $\sim 2500$  pC/N has been obtained along their pseudocubic  $\langle 001 \rangle$  direction. From crystallographic considerations and their hysteresis-free strain vs electric field behavior, it is suggested that non-180° domain wall motion does not contribute to the piezoelectric response for  $\langle 001 \rangle$  oriented rhombohedral single crystals (below the field-forced rhombohedral to tetragonal transition), because there is no driving force for non-180° domain wall motion.

Therefore, oriented relaxor-PT films are interesting from the viewpoint of piezoelectric films, since in these materials non-180° domain wall motion is not necessary to obtain high piezoelectric responses. Although there are several reports on the deposition and properties of relaxor-PT films, most of these studies focus on materials such as PMN-PT that have

relatively low transition temperatures (typically  $< 200$  °C).<sup>11–13</sup> For MEMS applications, since temperature stability of the piezoelectric properties is also important, ferroelectrics with high transition temperatures are attractive. Of the known relaxor ferroelectric- $\text{PbTiO}_3$  solid solutions,  $(1-x)\text{Pb}(\text{Yb}_{1/2}\text{Nb}_{1/2})\text{O}_3-x\text{PbTiO}_3$  (PYbN-PT) has the highest transition temperature ( $\sim 360$  °C) near the morphotropic phase boundary ( $x \sim 0.5$ ).<sup>14,15</sup> In PYbN-PT bulk ceramics, relaxor ferroelectric behavior at compositions in the range from  $x=0.2$  to 0.49 and remanent polarizations as high as  $32.8 \mu\text{C}/\text{cm}^2$  have been observed.<sup>16,17</sup> The growth and ferroelectric properties of PYbN-PT epitaxial films have been reported by Bornand *et al.*<sup>18–20</sup> We have investigated the piezoelectric properties of PYbN-PT epitaxial films.<sup>21</sup> Since the piezoelectric properties of relaxor-PT single crystals depend on the orientation and composition, in this article the piezoelectric properties of epitaxial  $(1-x)\text{PYbN-}x\text{PT}$  ( $x=0.4, 0.5$ ) films with (001) and (111) orientations were characterized.

## II. EXPERIMENTAL PROCEDURE

PYbN-PT films and  $\text{SrRuO}_3$  bottom electrodes were prepared by pulsed laser deposition on (100)  $\text{LaAlO}_3$ , (100)  $\text{SrTiO}_3$ , and (111)  $\text{SrTiO}_3$  single crystal substrates (MTI corporation). (Note that in this article, the Miller indices of  $\text{LaAlO}_3$ ,  $\text{SrRuO}_3$ , and PYbN-PT are given in terms of a pseudocubic unit cell.) A KrF excimer laser (Lambda Physik Compex 102) with a 248 nm wavelength was used to ablate the target materials. The specific deposition conditions of the  $\text{SrRuO}_3$  bottom electrode and PYbN-PT films are given in Table I.  $\text{SrRuO}_3$  bottom electrodes were deposited using stoichiometric  $\text{SrRuO}_3$  ceramic targets (Target Materials Inc.). Details on the epitaxial growth of  $\text{SrRuO}_3$  films are given elsewhere.<sup>19,22</sup> PYbN-PT films were deposited using sintered ceramics of PYbN-PT with (50/50) and (60/40) compositions, including 25 wt % excess PbO to compensate for lead loss during growth.<sup>11</sup> Oxygen and ozone gases were

TABLE I. Deposition conditions for SrRuO<sub>3</sub> and PYbN-PT epitaxial films.

	SrRuO <sub>3</sub>	PYbN-PT
Temperature	730–760 °C	600–680 °C
Atmosphere	100% O <sub>2</sub>	10% O <sub>3</sub> –90% O <sub>2</sub>
Pressure	200 mTorr	400 mTorr
Laser energy density	1.2 J/cm <sup>2</sup>	1–5 J/cm <sup>2</sup>
Laser repetition rate	10 Hz	2–5 Hz
Target	Stoichiometric	25 wt % excess PbO
Target to substrate distance	80 mm	45 mm
Thickness	300 nm	1000 nm

introduced to the deposition chamber using a commercial ozone generator (PCI). After deposition, the films were quickly cooled in a 200 Torr oxygen/ozone atmosphere to room temperature.

The crystalline phases and structure of the films were characterized by x-ray diffraction (XRD) using Cu *K*α radiation.  $\theta$ – $2\theta$ ,  $\omega$ , and  $\phi$  scans were performed using a Scintag Pad V diffractometer and an X'PERT Phillips four circle diffractometer. To characterize electrical properties, Au/Cr dot electrodes (area = 0.040–0.128 mm<sup>2</sup>) were fabricated by thermal evaporation and photolithographic processing. The dielectric constant and loss were determined using an impedance analyzer (Hewlett Packard 4192A). Polarization hysteresis loops were measured by a Radiant Technologies RT66A standard ferroelectrics tester at 100 Hz. The piezoelectric properties of PYbN-PT films were characterized in terms of effective piezoelectric transverse coefficients ( $e_{31,f}$ ). Since thin films are clamped on a substrate, the directly measured piezoelectric coefficient of the thin films is not the free piezoelectric coefficient but an effective coefficient.<sup>1,2,3</sup> The  $e_{31,f}$  coefficient for thin films is

$$e_{31,f} = \frac{d_{31}}{s_{11}^E + s_{12}^E}, \quad (1)$$

where  $d_{31}$  is the transverse piezoelectric coefficient (C/N) and  $s_{ij}^E$  are the elastic compliance coefficients of the film (N/m<sup>2</sup>) at constant electric field. The value of the  $e_{31,f}$  coefficient calculated by Eq. (1) using bulk ceramic data for PZT (52/48) is  $-9.6$  C/m<sup>2</sup>.<sup>24</sup> To date, the highest value of the  $e_{31,f}$  coefficient reported in PZT thin films is  $-12$  C/m<sup>2</sup>.<sup>2</sup>

The  $e_{31,f}$  coefficients were measured using the wafer flexure method described previously.<sup>25,26</sup> For the measurement, the PYbN-PT coated substrates were glued to a 3 in. (100) Si wafer. The Si wafer was suspended over a cavity and flexed periodically by changing the pressure inside the cavity. The biaxial stress generated in the film induced a charge via the piezoelectric effect. The charge and the strain generated at the film surface were measured by a lock-in amplifier (Model 7260 EG&G Instrument) and a strain indicator (Model 3800, Vishay measurement) using a strain gauge (KFG-1N-120-C1-11L3M3R, Omega Engineering Inc.) attached to the samples. The  $e_{31,f}$  is determined by the charge and the strain as

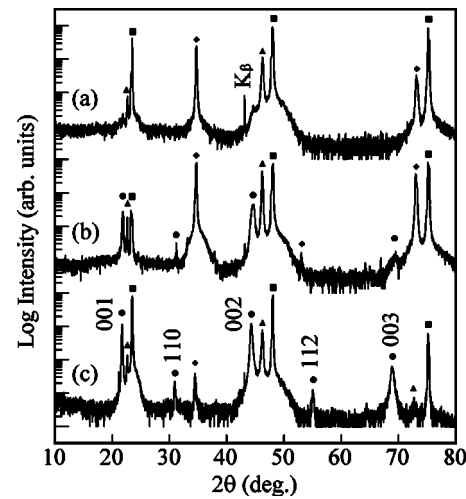


FIG. 1. XRD patterns of PYbN-PT (50/50) films deposited on (100) SrRuO<sub>3</sub>/(100) LaAlO<sub>3</sub> substrates. The (100) SrRuO<sub>3</sub>/(100) LaAlO<sub>3</sub> substrates were annealed at 700 °C in vacuum for (a) 1, (b) 10, and (c) 40 min. ●: Perovskite PYbN-PT; ▲: SrRuO<sub>3</sub>; ■: LaAlO<sub>3</sub>; and ◆: pyrochlore.

$$e_{31,f} = \frac{D_3}{x_1 + x_2}, \quad (2)$$

where  $x_1$  and  $x_2$  are the in-plane strain components and  $D_3$  is the induced dielectric displacement (C/m<sup>2</sup>).<sup>1,2,3</sup>

### III. RESULTS AND DISCUSSION

#### A. Phases and structure

Optimization of the growth conditions for PYbN-PT epitaxial films was performed on (100) SrRuO<sub>3</sub>/(100) LaAlO<sub>3</sub> substrates using the (50/50) composition target. In the deposition of Pb based perovskite films, the formation of a pyrochlore phase is common and is mainly caused by either low growth temperatures or lead deficiency. In PYbN-PT epitaxial films, this was also observed. However, another factor controlling pyrochlore formation was also found. Figure 1 shows  $\theta$ – $2\theta$  XRD patterns of PYbN-PT films deposited on (100) SrRuO<sub>3</sub>/(100) LaAlO<sub>3</sub> substrates that were annealed at 700 °C in vacuum ( $<1 \times 10^{-5}$  Torr) for various times. Subsequently, the PYbN-PT films were deposited using the same conditions (a substrate temperature of 620 °C, a deposition pressure of 300 mTorr, a laser repetition rate of 6 Hz, and a target to substrate distance of 55 mm). As can be seen in Fig. 1, the phase of the film changes from pyrochlore to perovskite with an increase in the SrRuO<sub>3</sub> annealing time. A perovskite PYbN-PT film with high (001) orientation was obtained after vacuum annealing the substrate for 40 min. However, no significant difference in the XRD profile for the SrRuO<sub>3</sub> itself was observed before and after the annealing. It is possible that the differences were associated either with surface reconstruction [as has been reported for

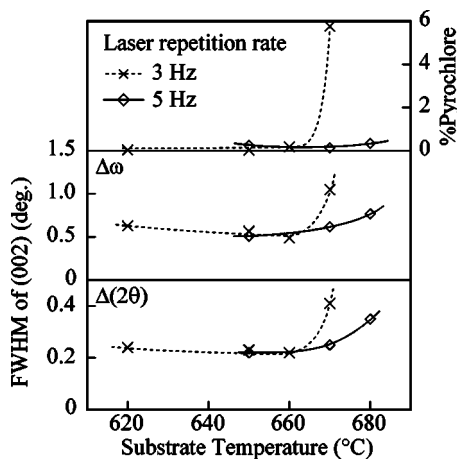


FIG. 2. The quantity of pyrochlore phase and FWHM of PYbN-PT 002 reflection in the  $\theta$ - $2\theta$  scan and  $\omega$  scan (rocking curve) for PYbN-PT films deposited at various temperature and laser repetition rates of 3 and 5 Hz.

(100) SrTiO<sub>3</sub> single crystals<sup>27</sup>] or volatility of ruthenium oxide.<sup>28</sup> Consequently, subsequent growths were performed on annealed SrRuO<sub>3</sub> electrodes.

To optimize the growth conditions of the PYbN-PT films, the films were deposited at various substrate temperatures and laser frequencies. The deposition pressure and target to substrate distance were fixed at 400 mTorr and 45 mm, respectively. (100) SrRuO<sub>3</sub>/(100) LaAlO<sub>3</sub> substrates were annealed at 790 °C for 40 min just before each deposition of a-PYbN-PT film. The PYbN-PT films were characterized by XRD. The growth rates at laser frequencies of 3 and 5 Hz were 60 and 90 nm/min, respectively. Figure 2 shows the quantity of pyrochlore phase and the full width at half-maximum (FWHM) for the PYbN-PT (002) reflection in the  $\theta$ - $2\theta$  and  $\omega$  (rocking curve) scans as a function of the substrate temperature. The quantity of pyrochlore phase was estimated from the ratio of the diffraction peak intensities of the pyrochlore phase (34.7°) to PYbN-PT (002). The (001) PYbN-PT films were obtained at deposition temperatures up to 670 °C at a 3 Hz pulse rate. At 670 °C, however, the quantity of pyrochlore phase increased to 6%. The FWHM in the  $\theta$ - $2\theta$  and  $\omega$  scans also increased. Therefore, for growth with a 3 Hz pulse rate, perovskite PYbN-PT was favored up to 660 °C. In contrast, (001) PYbN-PT films with <0.5% pyrochlore phase could be achieved for temperatures below 680 °C at a 5 Hz pulse rate. Thus higher growth rates are required to obtain perovskite PYbN-PT at higher temperatures. These results are consistent with increased Pb volatilization at higher temperatures favoring pyrochlore phase formation. For higher laser pulse rates, the delivery rate for PbO was sufficiently high that the perovskite phase could be stabilized to higher temperature.

In Fig. 2, (001) PYbN-PT films with the best crystalline quality were obtained at 650–660 °C. Figure 3(a) shows a  $\theta$ - $2\theta$  XRD pattern for a (001) PYbN-PT film deposited at 650 °C and a laser repetition rate of 3 Hz. Although small peaks were present at 31.0° and 34.7° [corresponding to PYbN-PT (110) and a pyrochlore phase, respectively], the intensity ratio of the small peaks to the PYbN-PT (002) peak was <0.1%. Using this growth condition, PYbN-PT

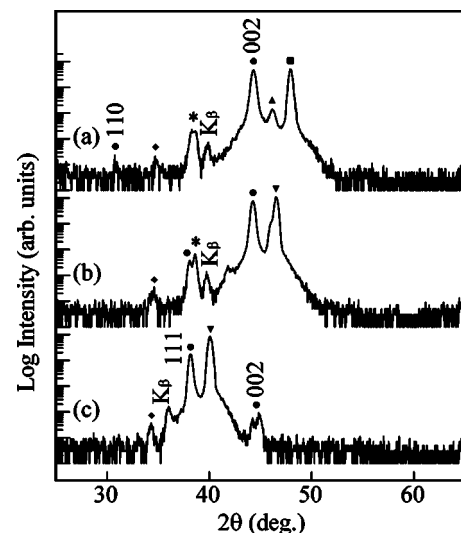


FIG. 3.  $\theta$ - $2\theta$  XRD patterns of (a) a (001) PYbN-PT film on (100) SrRuO<sub>3</sub>/(100) LaAlO<sub>3</sub>, (b) a (001) PYbN-PT film on (100) SrRuO<sub>3</sub>/(100) SrTiO<sub>3</sub>, and (c) a (111) PYbN-PT film on (111) SrRuO<sub>3</sub>/(111) SrTiO<sub>3</sub>. The deposition temperatures were (a) 650, (b) 650, and (c) 620 °C. ●: Perovskite PYbN-PT; ▲: SrRuO<sub>3</sub>; ■: LaAlO<sub>3</sub>; ▼: SrTiO<sub>3</sub>; ◆: pyrochlore; and \*: Au top electrode.

(50/50) films were deposited on (100) SrRuO<sub>3</sub>/(100) SrTiO<sub>3</sub> and (111) SrRuO<sub>3</sub>/(111) SrTiO<sub>3</sub> substrates. Since it is reported that the piezoelectric properties of films may depend on the substrate due to differences in the thermal expansion coefficient,<sup>29</sup> not only (100) SrRuO<sub>3</sub>/(100) LaAlO<sub>3</sub> but (100) SrRuO<sub>3</sub>/(100) SrTiO<sub>3</sub> was used. As shown in Fig. 3(b), (001) PYbN-PT films with good phase purity were obtained on (100) SrRuO<sub>3</sub>/(100) SrTiO<sub>3</sub> substrates also. However, PYbN-PT films deposited on (111) SrRuO<sub>3</sub>/(111) SrTiO<sub>3</sub> substrates were not well crystallized. In a  $\theta$ - $2\theta$  XRD pattern of the film, only small diffraction peaks from the film were observed. It was found that (111) PYbN-PT films with good phase purity could be obtained at 600–620 °C as shown in Fig. 3(c). Thus, the optimum growth temperature depended on the substrates.

The in-plane orientation of the (001) and (111) PYbN-PT films shown in Fig. 3 was investigated by  $\phi$  XRD scans. The (101) reflections of PYbN-PT, LaAlO<sub>3</sub>, and SrTiO<sub>3</sub> were selected for this measurement. The results are shown in Fig. 4. Epitaxial growth of PYbN-PT films was confirmed on each of the substrates. In (001) PYbN-PT on (100) SrRuO<sub>3</sub>/(100) LaAlO<sub>3</sub> and (111) PYbN-PT on (111) SrRuO<sub>3</sub>/(111) SrTiO<sub>3</sub>, weak peaks corresponding to misoriented grains (45° and 60° rotations, respectively) were observed. The amount estimated from the intensity ratio of the diffraction peaks was less than 1%.

In the same way, (001) and (111) PYbN-PT epitaxial films with (60/40) composition were prepared on (100) SrRuO<sub>3</sub>/(100) LaAlO<sub>3</sub>, (100) SrRuO<sub>3</sub>/(100) SrTiO<sub>3</sub>, and (111) SrRuO<sub>3</sub>/(111) SrTiO<sub>3</sub> substrates. The quantity of pyrochlore phase and FWHM in  $\theta$ - $2\theta$ ,  $\omega$ , and  $\phi$  scans for the PYbN-PT (50/50) and (60/40) epitaxial films are summarized in Table II. In the  $\theta$ - $2\theta$  and  $\omega$  scans for the (111) films, the PYbN-PT (111) reflection was used. The FWHM shown for SrTiO<sub>3</sub> is indicative of the instrumental resolution.

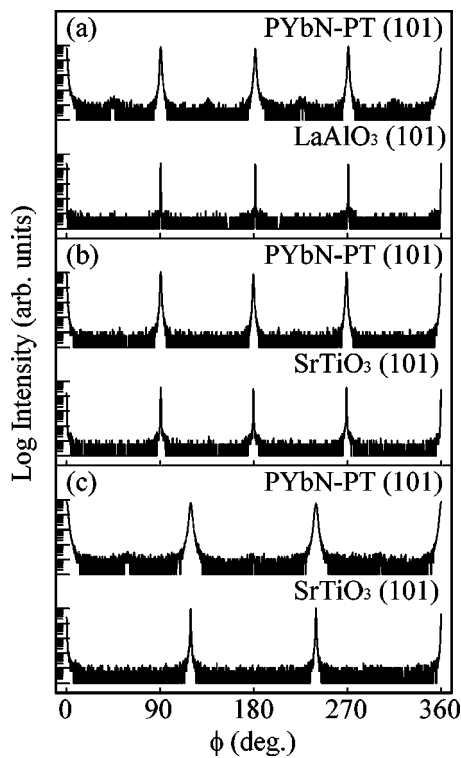


FIG. 4.  $\phi$  XRD scan profiles of the PYbN-PT films. (101) reflections of PYbN-PT, SrTiO<sub>3</sub>, LaAlO<sub>3</sub> were used. (a) A (001) PYbN-PT film on (100) SrRuO<sub>3</sub>/(100) LaAlO<sub>3</sub>, (b) a (001) PYbN-PT film on (100) SrRuO<sub>3</sub>/(100) SrTiO<sub>3</sub>, and (c) a (111) PYbN-PT film on (111) SrRuO<sub>3</sub>/(111) SrTiO<sub>3</sub>.

## B. Ferroelectric and dielectric properties

Figure 5 shows the polarization hysteresis loops for PYbN-PT (50/50) and (60/40) epitaxial films. Well-saturated hysteresis loops were observed for all films. The remanent polarization, dielectric constant, and dielectric loss for these films are listed in Table II. In both (50/50) and (60/40) compositions, (001) epitaxial films showed lower dielectric constants and higher remanent polarizations than (111) epitaxial films. It seems that in (111) epitaxial films, the polarization in some regions of the films is largely in-plane and is not switched by the applied electric field due to limited non-180° domain wall motion.<sup>19</sup> In both (001) and (111) epitaxial films, the (50/50) films have larger remanent polarization than the (60/40) films. The relatively high dielectric losses (5%–7%) are likely due to the domain wall motion, because the dielectric losses decreased to ~2% by applying a dc bias of 20 V.<sup>7,30</sup>

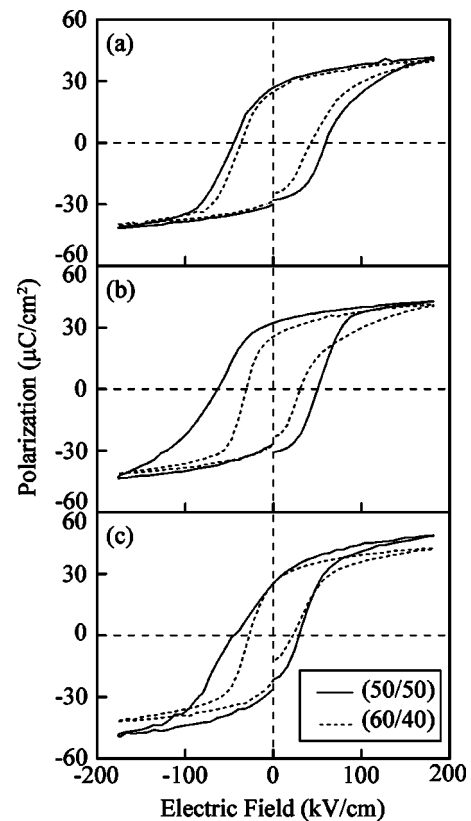


FIG. 5. Polarization hysteresis loops of PYbN-PT (50/50) and (60/40) films on (a) (100) SrRuO<sub>3</sub>/(100) LaAlO<sub>3</sub>, (b) (100) SrRuO<sub>3</sub>/(100) SrTiO<sub>3</sub>, and (c) (111) SrRuO<sub>3</sub>/(111) SrTiO<sub>3</sub>.

Figure 6 shows the temperature dependence of the dielectric constant and loss for the (001) PYbN-PT epitaxial films on (100) SrRuO<sub>3</sub>/(100) LaAlO<sub>3</sub>. This measurement was performed during heating. For (50/50) and (60/40) compositions, the dielectric constant has a maximum near 380 and 320 °C, respectively. The maximum dielectric constant (at 10 kHz) of the (50/50) film ( $\epsilon_r \sim 3200$ ) was higher than that of the (60/40) film ( $\epsilon_r \sim 1900$ ). The behavior of the dielectric constant is consistent with the data obtained in bulk ceramics with the same composition.<sup>16,17</sup> From these results, it is suggested that the B-site stoichiometry of the (50/50) and (60/40) films was nearly that of the targets.

## C. Piezoelectric properties

Prior to measurements of the piezoelectric coefficients, PYbN-PT films were poled with a dc electric field at room

TABLE II. The crystalline quality, electrical properties, and piezoelectric  $e_{31f}$  coefficient for the  $(1-x)$ PYbN- $x$ PT epitaxial films.

Substrate	Orientation	$x$	FWHM $\theta-2\theta, \omega, \phi$	% pyrochlore	$\epsilon_r, \tan \delta$ at 1 kHz	$P_r$ ( $\mu\text{C}/\text{cm}^2$ )	$e_{31f}$ ( $\text{C}/\text{m}^2$ )
LaAlO <sub>3</sub>	001	0.5	0.23°, 0.59°, 0.99°	<0.1	900, 0.06	29	-14
SrTiO <sub>3</sub>	001	0.5	0.25°, 0.52°, 0.74°	<0.1	1000, 0.04	30	-12
SrTiO <sub>3</sub>	111	0.5	0.26°, 0.89°, 1.76°	<0.2	1300, 0.05	25	-3.3
LaAlO <sub>3</sub>	001	0.4	0.21°, 0.53°, 0.96°	0.1	950, 0.04	27	-10
SrTiO <sub>3</sub>	001	0.4	0.24°, 0.56°, 0.91°	0.1	1000, 0.05	26	-9
SrTiO <sub>3</sub>	111	0.4	0.18°, 0.71°, 1.48°	0.2	1300, 0.07	24	-2.5
	100	SrTiO <sub>3</sub>	0.18°, 0.20°, 0.23°				

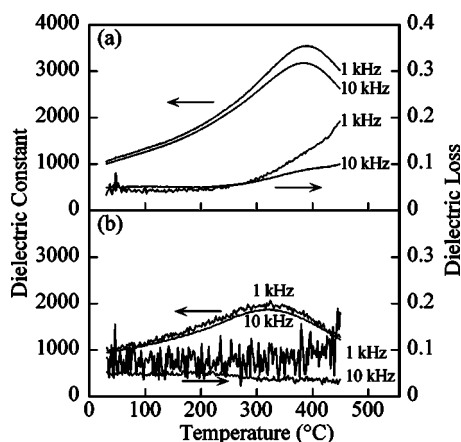


FIG. 6. The temperature dependence of the dielectric constant and loss for the (001) PYbN-PT films with (a) (50/50) and (b) (60/40) compositions on (100) SrRuO<sub>3</sub>/(111) LaAlO<sub>3</sub>. The cooling rate was 2 °C/min.

temperature. Figure 7 shows the variation of the  $e_{31,f}$  coefficient for the (001) PYbN-PT (50/50) film on (100) SrRuO<sub>3</sub>/(100) LaAlO<sub>3</sub> as functions of the poling electric field and time. There was significant asymmetry in the  $e_{31,f}$  coefficient as a function of the poling direction. The  $e_{31,f}$  coefficient after poling with the negative electric field was almost constant. In contrast, when poled with a positive electric field, the  $e_{31,f}$  coefficient increased with poling electric field and time. However, the maximum  $e_{31,f}$  coefficient after poling with a positive electric field was lower than that with a negative electric field. The asymmetric behavior of the  $e_{31,f}$  coefficient can be explained by the internal bias electric field of the films as reported for sputtered PZT films.<sup>26,31</sup> As shown in Fig. 5(a), the hysteresis loops for the (001) PYbN-PT (50/50) film were shifted 7 kV/cm along the electric field axis, suggesting an internal bias electric field.

Similar asymmetric behavior of the  $e_{31,f}$  coefficient was observed in other PYbN-PT films. When the hysteresis loops were shifted towards the positive direction, the  $e_{31,f}$  coefficient after poling with the negative electric field were higher than those with the positive electric field. The highest  $e_{31,f}$  coefficient obtained for each of the PYbN-PT films is

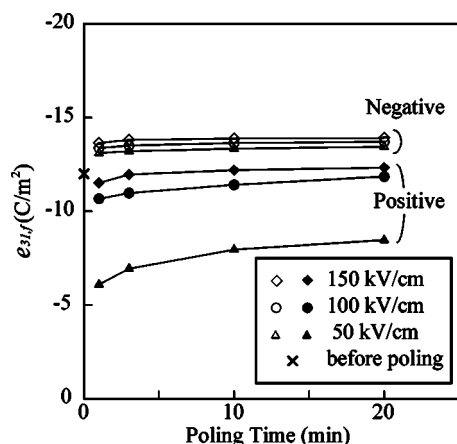


FIG. 7. The  $e_{31,f}$  coefficient for a (001) PYbN-PT (50/50) film on (100) SrRuO<sub>3</sub>/(100) LaAlO<sub>3</sub> as a function of the poling electric field and time.

summarized in Table II. In both (50/50) and (60/40) compositions, the  $e_{31,f}$  coefficients for the (111) films were much lower than those for the (001) films, even though there are no large differences in the dielectric constant and remanent polarizations. This result is comparable to that previously reported for relaxor-PT single crystals.<sup>10</sup>

Although it has been suggested previously that substrates of different composition markedly affect the piezoelectric properties of PMN-PT epitaxial films,<sup>29</sup> only small differences in the  $e_{31,f}$  coefficient were observed between (001) LaAlO<sub>3</sub> and (001) SrTiO<sub>3</sub> substrates. Since thick SrRuO<sub>3</sub> bottom electrodes (300 nm) and PYbN-PT films (1 μm) were used in this work, and no shift of the transition temperature was observed (as shown in Fig. 6), it is expected that stresses associated with lattice mismatch are relieved for these PYbN-PT films.

In both (001) and (111) epitaxial films, the (50/50) films exhibited higher  $e_{31,f}$  coefficients than the (60/40) films. Thus, the highest  $e_{31,f}$  coefficient was obtained on (001) PYbN-PT (50/50) epitaxial films.

#### IV. CONCLUSIONS

The epitaxial growth and transverse piezoelectric properties of  $(1-x)\text{Pb}(\text{Yb}_{1/2}\text{Nb}_{1/2})\text{O}_3-x\text{PbTiO}_3$  ( $x=0.4,0.5$ ) films deposited by pulsed laser deposition was examined. It was found that the surface condition of the SrRuO<sub>3</sub> bottom electrodes, as well as growth temperature and lead deficiency, affected the phase formation of PYbN-PT. (001) PYbN-PT perovskite thin films were obtained for a wide range of deposition rates (60–90 nm/min) and temperatures (620–680 °C) after vacuum annealing the SrRuO<sub>3</sub> bottom electrodes. In both (50/50) and (60/40) compositions, (001) PYbN-PT epitaxial films with good crystalline quality were obtained on (100) SrRuO<sub>3</sub>/(100) LaAlO<sub>3</sub> and (100) SrRuO<sub>3</sub>/(100) SrTiO<sub>3</sub> substrates at 650 °C, whereas the optimum growth temperature of (111) PYbN-PT epitaxial films on (111) SrRuO<sub>3</sub>/(111) SrTiO<sub>3</sub> substrates was 600–620 °C. The (001) films exhibited higher remanent polarizations and piezoelectric  $e_{31,f}$  coefficients than the (111) films. The transition temperatures of the (50/50) and (60/40) films were near 380 and 320 °C, respectively (similar to data obtained on bulk ceramics with equivalent composition). An  $e_{31,f}$  coefficient of  $-14\text{ C/m}^2$  and a remanent polarization of  $\sim 30\ \mu\text{C/cm}^2$  were obtained on (001) PYbN-PT epitaxial films with the (50/50) composition (near the morphotropic phase boundary).

#### ACKNOWLEDGMENTS

The authors are grateful to B. Jones and M. Angelone for their cooperation in the ceramic target synthesis and texture analyses, respectively. Support for this work was provided by the Office of Naval Research (U.S.) under Contract No. N00014-98-1-0527.

<sup>1</sup> P. Muralt, J. Micromech. J. Micromech. Microeng. **10**, 136 (2000).

<sup>2</sup> P. Muralt, IEEE Trans. Ultrason. Ferroelectr. Freq. Control **47**, 903 (2000).

<sup>3</sup> D. Bishop, A. Heuer, and D. Williams, MRS Bull. **26**, 282 (2001).

<sup>4</sup> T. Tsuchiya, T. Itoh, G. Sakai, and T. Suga, J. Ceram. Soc. Jpn. **104**, 159 (1996).

- <sup>5</sup>E. Cattan, T. Haccart, G. Velu, D. Remiens, C. Bergaud, and L. Nicu, *Sens. Actuators A* **74**, 60 (1998).
- <sup>6</sup>J. Kanno, S. Fujii, T. Kamada, and R. Takayama, *Appl. Phys. Lett.* **70**, 1378 (1997).
- <sup>7</sup>Q. M. Zhang, H. Wang, N. Kim, and L. E. Cross, *J. Appl. Phys.* **75**, 454 (1994).
- <sup>8</sup>S. Trolrier-McKinstry, P. Aungkavattana, F. Chu, J. Lacey, J.-P. Maria, J. F. Shepard, T. Su, and F. Xu, *Mater. Res. Soc. Symp. Proc.* **493**, 59 (1998).
- <sup>9</sup>F. Xu, S. Trolrier-McKinstry, W. Ren, B. Xu, Z.-L. Xie, and J. Hemker, *J. Appl. Phys.* **89**, 1336 (2001).
- <sup>10</sup>S. E. Park and T. R. ShROUT, *J. Appl. Phys.* **82**, 1804 (1997).
- <sup>11</sup>J. P. Maria, W. Hackenberger, and S. Trolrier-McKinstry, *J. Appl. Phys.* **84**, 5147 (1998).
- <sup>12</sup>J. H. Park, F. Xu, and S. Trolrier-McKinstry, *J. Appl. Phys.* **89**, 568 (2001).
- <sup>13</sup>Z. Kighelman, D. Damjanovic, and N. Setter, *J. Appl. Phys.* **89**, 1393 (2001).
- <sup>14</sup>S. Zhang, P. W. Rehrig, C. Randall, and T. R. ShROUT, *J. Cryst. Growth* **234**, 415 (2002).
- <sup>15</sup>T. Mitsui and E. Nakamura, *Landolt-Börnstein* (Springer, Berlin, 1990), Vol. III/28.
- <sup>16</sup>T. Yamamoto and S. Ohashi, *Jpn. J. Appl. Phys., Part 1* **34**, 5349 (1995).
- <sup>17</sup>H. Lim, H. J. Kim, and W. K. Choo, *J. Appl. Phys.* **34**, 5449 (1995).
- <sup>18</sup>V. Bornand and S. Trolrier-McKinstry, *Thin Solid Films* **370**, 70 (2000).
- <sup>19</sup>V. Bornand and S. Trolrier-McKinstry, *J. Appl. Phys.* **87**, 3958 (2000).
- <sup>20</sup>V. Bornand, S. Trolrier-McKinstry, K. Takemura, and C. A. Randall, *J. Appl. Phys.* **87**, 3965 (2000).
- <sup>21</sup>T. Yoshimura and S. Trolrier-McKinstry, *J. Cryst. Growth* **229**, 445 (2001).
- <sup>22</sup>J. P. Maria, S. Trolrier-McKinstry, D. G. Schlom, M. E. Hawley, and G. W. Brown, *J. Appl. Phys.* **83**, 4373 (1998).
- <sup>23</sup>M.-A. Dubois and P. Mural, *Sens. Actuators A* **77**, 106 (1999).
- <sup>24</sup>T. Mitsui and S. Nomura, *Landolt-Börnstein* (Springer, Berlin, 1981) Vol. III/16, p. 123.
- <sup>25</sup>J. F. Shepard, Jr., P. J. Moses, and S. Trolrier-McKinstry, *Sens. Actuators A* **71**, 133 (1998).
- <sup>26</sup>J. F. Shepard, Jr., F. Chu, I. Kanno, and S. Trolrier-McKinstry, *J. Appl. Phys.* **85**, 6711 (1999).
- <sup>27</sup>M. Lippmaa, M. Kawasaki, A. Ohtomo, T. Sato, M. Iwatsuki, and H. Kounuma, *Appl. Surf. Sci.* **130–132**, 582 (1998).
- <sup>28</sup>W. Pan and S. B. Desu, *J. Vac. Sci. Technol. B* **12**, 3208 (1994).
- <sup>29</sup>V. Nagarajan S. P. Alpay, C. S. Ganpule, B. K. Nagarai, S. Aggarwal, E. D. Williams, A. L. Roytburd, and R. Ramesh, *Appl. Phys. Lett.* **77**, 438 (2000).
- <sup>30</sup>O. Lohse, M. Grossmann, D. Bolten, U. Boettger, and R. Waser, *Mater. Res. Soc. Symp. Proc.* **655**, CC7.6.1 (2001).
- <sup>31</sup>A. Kholkin, E. Colla, K. Brooks, P. Mural, M. Kohli, T. Maeder, D. Taylor, and N. Setter, *Microelectron. Eng.* **29**, 261 (1995).